ADVANCED FUNCTIONAL MATERIALS
www.afm-journal.de

The Relation Between Molecular Packing or Morphology and Chemical Structure or Processing Conditions: the Effect on Electronic Properties

Pramod Kumar, Kammasandra Nanajunda Shivananda, Wojciech Zajączkowski, Wojciech Pisula, Yoav Eichen, and Nir Tessler**

In the past few decades, mainly two kind of organic semiconductors, namely small molecules and polymers, have been dealt with. It turns out that the difference between these two categories in terms of charge carrier transport arises from the potentially different morphologies and the molecular packing. There are many studies showing the effect of the chemical structure on the electronic properties. However, in this study, the focus is on the role of processing conditions which is found to be of at least equal importance. To study a range of morphologies and packing in as similar molecules, two systems prepared by "Click"-type chemistry are chosen, with the major difference between them being the replacement of a flat unit with one that introduces a slight twist to the aromatic skeleton. Through AFM and X-ray studies, it is shown that the molecule with the potentially flat geometry can exhibit a high degree of π–π stacking, leading to morphologies ranging from polycrystalline to single crystals while the other is always in the amorphous film state. The transport properties are compared using organic field effect transistor (OFETs) in both top and bottom contact configurations.

1. Introduction

Over the past decade π-conjugated small molecule and polymers have generated considerable attention because of their possible applications in organic electronics such as light-emitting diodes,[1] organic lasers,[2] field-effect transistors (FETs),[3] sensors,[4] and photovoltaic cells.[5] It has been shown that the differences between these two categories are mainly due to the way the molecules arrange themselves in thin films. The main advantages of using small molecules is that these can be synthesized in high purity and precision which facilitates high order and often result in high charge carrier field-effect mobility. When crystallization takes place, especially in the case of single crystals, the tight packing would also improve the durability under ambient conditions.[6] The traditional disadvantage of small molecules is in the required processing which is mostly done through vapor-phase deposition that is less amendable to low-cost roll-to-roll deposition, which seems to be the ultimate goal for producing organic electronics. Other disadvantages include the existence of grain boundaries and the lower mechanical flexibility of the layers. Moving to polymers, they come with advantages like solution processing which is desirable for large area applications. Their major disadvantages lie in their inherently lower purity and larger disorder in thin films which is the main cause of low charge-carrier mobility in most systems. Recent work indicates that both fields of small molecules and polymers are merging with the emergence of solution processable small molecules and high mobility π-stacked polymers.[7] Solution processability of small molecules is normally achieved by attaching bulky side-groups to small molecules while in polymers the charge-carrier mobility has reached as high as 8 $cm^2\ V^{-1}\ s^{-1}$ by structurally modifying the polymers in a way that they can form closely packed structures in films.[8] As the differences are no longer directly associated with the length of the molecule and since the chemical structure is known to play a major role, it is beneficial to study the effect of different processing procedures applied to structurally similar molecules of almost same size.

Dr. P. Kumar, Prof. N. Tessler
Nanoelectronics Center, Department of Electrical Engineering
Technion – Israel Institute of Technology
Technion City, 32000, Haifa, Israel
E-mail: nir@ee.technion.ac.il
Dr. K. N. Shivananda, Prof. Y. Eichen
Schulich Faculty of Chemistry, Technion – Israel Institute of Technology
Technion City, 32000, Haifa, Israel
E-mail: chryoav@tx.technion.ac.il
W. Zajączkowski, Dr. W. Pisula
Max Planck Institute for Polymer Research
Ackermannweg 10,
55128, Mainz, Germany

DOI: 10.1002/adfm.201303571

2. Results and Discussion

2.1. Molecular Structure

In order to find two molecules that are best suited for the current study we opted to use "click"-type chemistry. Such approach is known to have a very broad scope and in fact nature utilizes "click"-type chemistry when dealing with the production of the

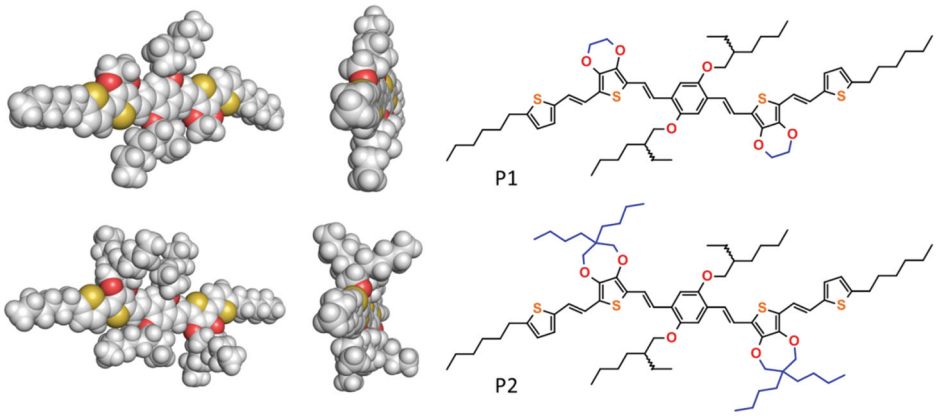

Figure 1. An energy minimized (DFT, B3LYP/6–31G(d)) structure of **P1** and **P2**, showing the planer structure of **P1** and the protruding bulky groups of **P2**.

molecular basis of diversity, polynucleic acids and proteins.[9] Adopting such a strategy to the preparation of organic electronic materials is expected to allow us to build complex π-conjugated structures and fine-tune these materials in a rather simple and straightforward way. Recently, it has been applied to the preparation and optimization of π-conjugated materials.[10,11] We have reported on the solution synthesis of oligo homo- and hetero-π-conjugated peptides and their optical and electrical properties.[12] Here, we had applied the LEGO-like sequence independent and bio-inspired "click" procedure of double-bond formation to produce structurally controlled functional oligomers.[13] Using this protocol we were able to prepare two closely related molecules in which two 2,3-dihydrothieno[3,4-b][1,4]dioxine (EDOT) units of one oligomer, **P1**, are substituted by two 3,3-dibutyl-2,4-dihydrothieno[3,4-b][1,4]dioxepine groups in the second oligomer, **P2**, **Figure 1**. (**P1** and **P2**). The two butyl groups of the 2,4-dihydrothieno[3,4-b][1,4]dioxepine group in **P2** are located on a quaternary carbon atom. This causes them to extend perpendicular to the plane of the π-conjugated skeleton. This simple modification in the molecule is expected to reflect in its film forming properties and influence carrier transport. The bulky groups were expected to hinder the π–π stacking giving a kind of amorphous and semi crystalline morphology often found in polymers. As we show below, this strategy along with employing a range of film processing conditions allow us to examine a range of morphologies and packing structures and their influence on the electronic properties of the organic layers.

2.2. Processing and Morphologies

Thin films were prepared on SiO_2 and glass substrates and subsequently annealed at different temperatures, then characterized using UV-Vis spectroscopy and atomic force microscopy (AFM). The AFM images in **Figure 2** show films of **P1** and **P2** on SiO_2 substrates after annealing at different temperatures. The films, annealed at different temperatures, show a marked difference in morphology. **P1** films show a transition from different polycrystalline morphologies to what seems to be larger crystal structures at 150 °C. Annealing at higher temperatures show larger grain sizes due to the higher mobility of the molecules on the surface, as shown in Figure 2a–c. On the other hand, films of **P2** remain amorphous at all annealing temperatures, Figure 2d–f.

To gain more insight of the morphological differences between films made of these two oligomers we measured the UV-Vis absorption spectrum of both films on glass and in THF solutions. It has been shown previously that when there is a strong π–π interaction in thin films the absorption spectrum shows Davydov splitting[14] rendering the solid phase absorption different from the solution phase. **Figure 3**a,b show absorption spectrums for THF solutions and thin films of **P1** and **P2** respectively. While the amorphous P2 film shows some red shift, often associated with aggregates formation, the P1 film shows a different behavior. To better analyze the change in the absorption of P1 when going from solution to film we fitted both spectra to a sum of two Gaussians. The symbols represent the measured data and the lines represent the fits. For the solution phase we found the peaks to be at 500 nm and 540 nm and for the solid film phase at 490 nm and 570 nm. While the midpoint between the peaks shifts by about 10 nm to the red the widening of the distance between the peaks actually doubles from 40 nm in solution to 80 nm in the solid film phase. The above results are in good agreement with the P1 exhibiting strong π–π interactions along the stacking direction giving rise to enhanced splitting between the peaks and with P2 being hindered from stacking by its protruding bulky butoxy groups. This hindering leads to less ordered molecular orientation and to the amorphous nature of the resulting thin films of **P2**. X-ray data in Figure 3c shows peaks in case of **P1**, which is the manifestation of molecular order and stacking in thin films. In contrast, there is no sign of molecular order in **P2**.

To test and access various morphologies in films based on the **P1** molecule we extended the study above, showing larger crystals at 150 °C, to include also the effect of solution concentration. It was found that by changing the concentration of **P1** in the THF solutions, from which the films are made, the morphology of the films and the size and thickness of the

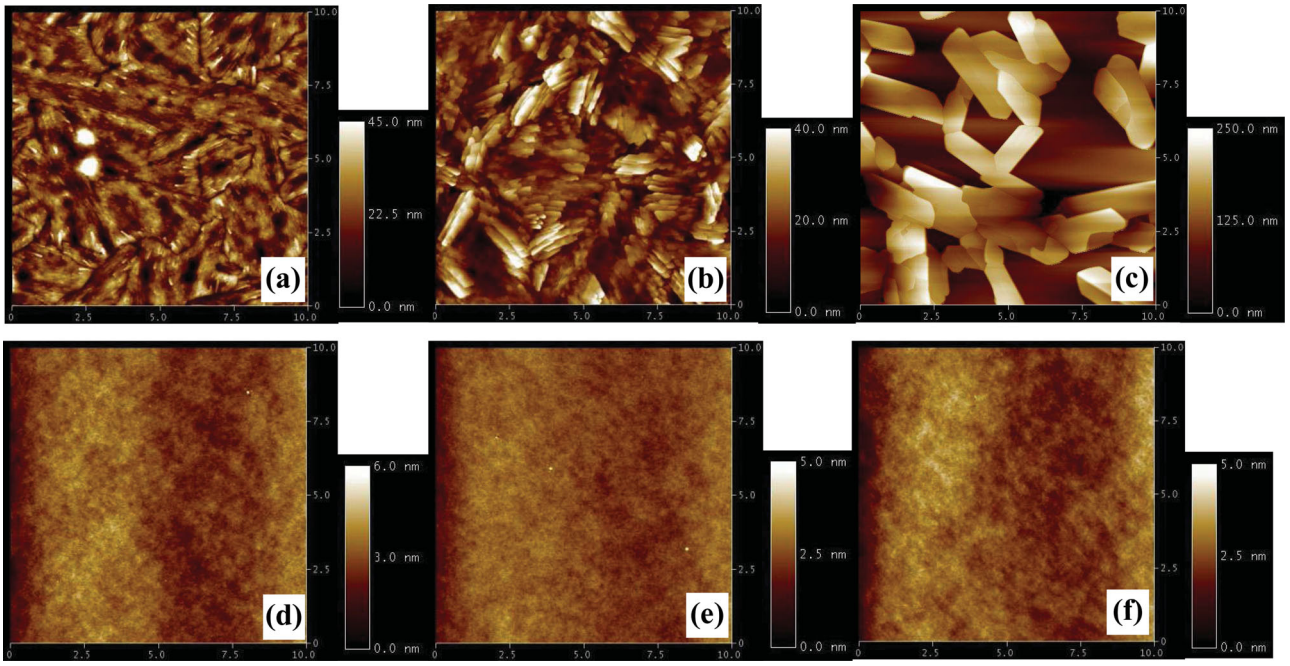

Figure 2. 10 μm × 10 μm AFM images of thin films of a–c) **P1** and d–f) **P2** on SiO_2 substrates prepared by 10 mg mL^{-1} solution. a,d) 60 °C; b,e) 90 °C; c,f) 150 °C.

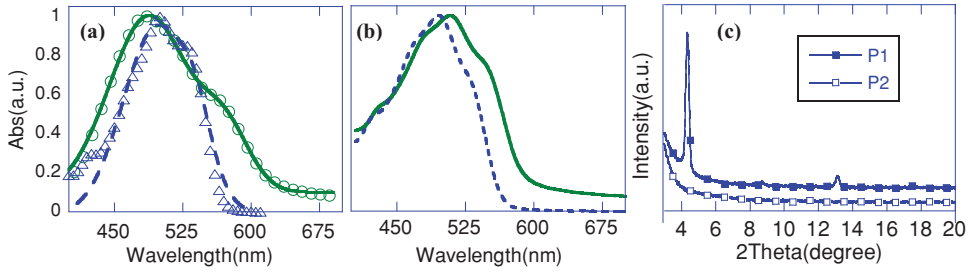

Figure 3. Normalized absorption spectra of a) **P1** and b) **P2**. The dashed and solid lines represent the absorption in THF solutions and thin films, respectively. For P1, the symbols are measured data and the solid line is the best fit to two Gaussian model. c) Shows X-ray diffraction of **P1** and **P2** films on SiO_2 substrates after annealing at 90 °C. The diffraction peaks in case of **P1** is the evidence of molecular packing while their absence in the case of **P2** indicates an amorphous film (**P1** X-ray pattern is shifted upward for better visualization).

larger crystals can be altered. **Figure 4** shows the AFM images of **P1** annealed at three different temperatures and with two different solution concentrations. The AFM images show that the average crystal size in films originating from dilute solutions is significantly smaller than in films formed from concentrated solutions. Figure 4c,f show the formation of rather large single crystals from the films. At low concentrations the larger crystals are independent and not attached to each other.

2.3. Single Crystals

As shown in Figure 4, at higher annealing temperatures we observe larger crystal formation which allows us to study single crystals. To do so we studied "films" originating from the low concentration solution (1 mg mL^{-1}) annealed at 150 °C for 3 h. **Figure 5** shows the topographic and phase images as well as a topographic cross section of a large crystal of **P1**. The phase image (Figure 5a) clearly shows a layer-by-layer growth which is attributed to the high mobility of the molecules on the SiO_2 surface at elevated temperatures. This growth mechanisms leads to a highly packed geometry giving rise to relatively large crystalline structures. The height profile in Figure 5c shows the thickness of the crystal which is about 14 nm. Annealing for different times show that crystals grow fully in 2–3 h (see Figure S3 and Table S1 in the Supporting Information). After 3 h of annealing, crystal thickness and length do not vary much and most crystals saturates to thickness of 14–15 nm.

Thickness of the crystals can also be controlled by changing the concentration of the solution (see Figure S1, Supporting Information). These crystals are directly grown on SiO_2 substrates, useful for developing single crystal transistor with lower dielectric/interface disorder. To gain an insight into the organization of **P1** on the surface and to understand the role of the annealing process on the evolution of its microstructure, grazing incidence wide-angle X-ray scattering (GI WAXS)

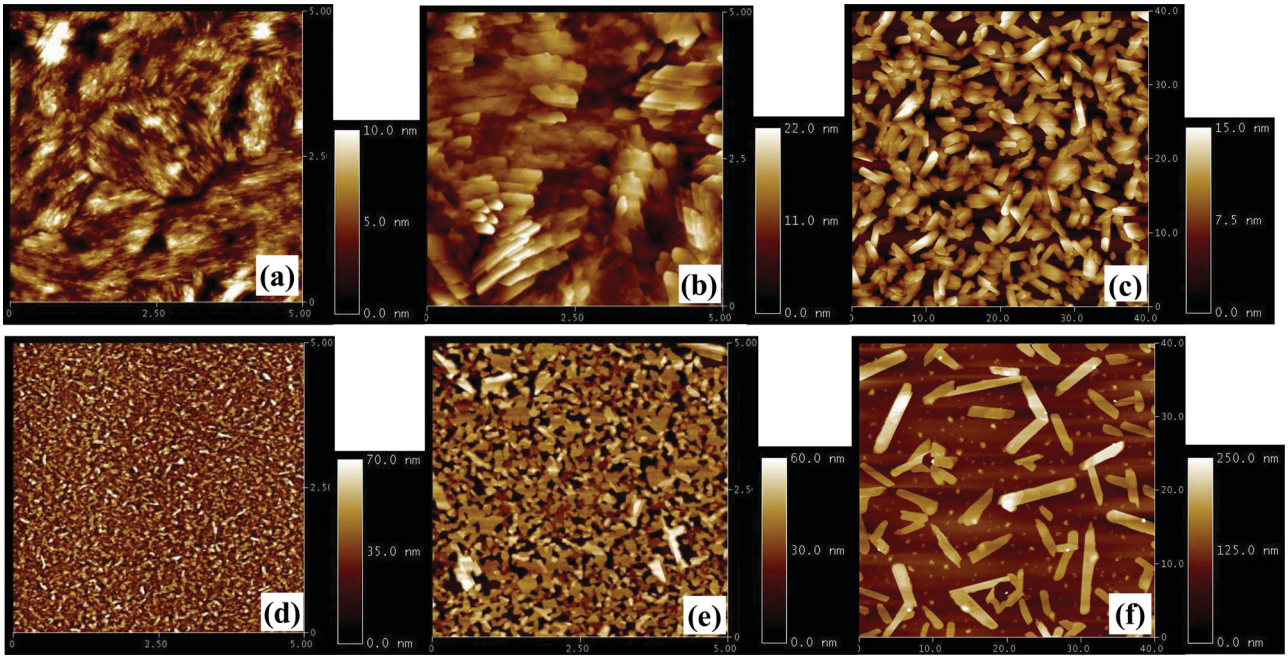

Figure 4. AFM scans of spin-coated thin films of **P1** grown on SiO_2 from two different THF solutions having concentrations: a–c) 10 mg mL^{-1} and d–f) 1 mg mL^{-1}. The films were annealed at different temperatures: a,d) 30 °C; b,e) 110 °C, and c,f) 150 °C. Note that (a,b,d,e) are 5 μm × 5 μm scans while (c,f) are 40 μm × 40 μm.

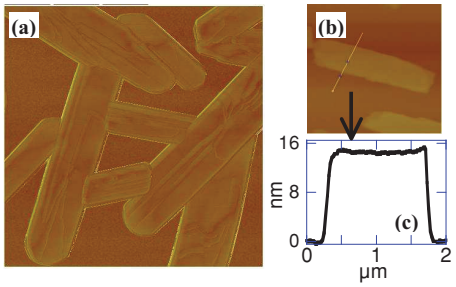

Figure 5. a) 5 μm × 5 μm AFM phase image showing the layer by layer growth in **P1** single crystals. b) AFM image of a independent signal crystal at 1 mg mL^{-1} solution concentration, c) Height profile of the cross section of a crystal in (b).

was performed. A characteristic pattern of the layer annealed at 120 °C is presented in **Figure 6**a. The large number of distinct reflections is typical of highly crystalline structures. Based on the location of the reflections, a packing model was derived which is based on edge-on arranged molecules with the *c*-axis (c = 20.95 Å) of the crystal aligned perpendicular to the surface (Figure 6c). Thereby, the π-stacking direction falls along the b-axis which is parallel to the surface, as indicated by the strong reflection at q_z = 0 $Å^{-1}$, $q_{x,y}$ = 1.78 $Å^{-1}$ (spacing of 3.53 Å between the π systems of adjacent molecules). This kind of organization is assumed to favor efficient transport of the charge carriers in film's plane as would be manifested in OFETs. Structure analysis of the patterns recorded for films annealed at other temperatures indicates that the molecular

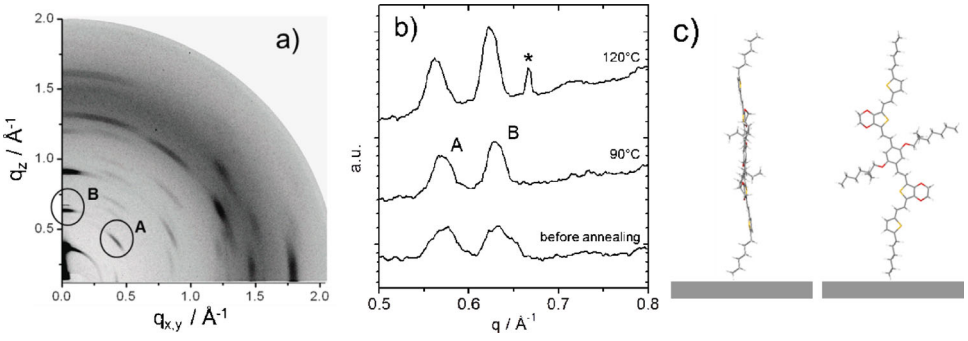

Figure 6. GIWAXS of **P1** after annealing at 120 °C a) experiment and b) integration of the GIWAXS patterns for samples annealed at different temperatures (A and B indicate reflections in (a), artifact in (b) is labeled by asterisk). c) Schematic illustration of edge-on arranged **P1** in two side views (optimization performed by DFT, B3LYP/6–31G(d)).

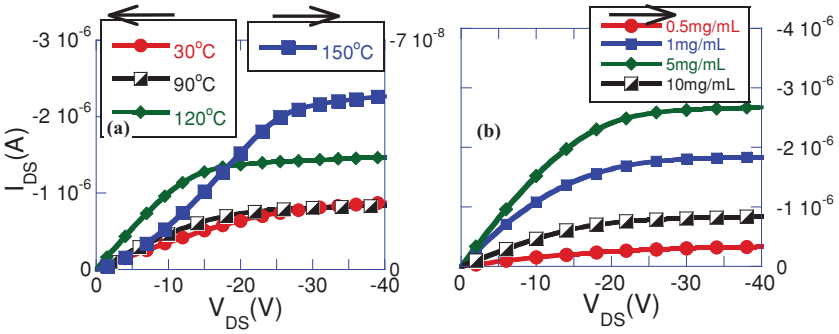

Figure 7. The output characteristics of **P1** OFETs at $V_{GS} = -10$ V. a) Thin films prepared at four different annealing temperatures with 10 mg mL^{-1} solution concentration (*y*-axis for 150 °C is on right). b) Thin films prepared at 90 °C with four different solution concentrations. The channel length and width were kept constant ($L = 100$ μm and $W = 35$ mm).

organization of **P1** on the surface is independent on annealing temperature, as the reflections do not change their positions. However, at higher annealing temperatures the order increases as indicated in Figure 6b for reflections A and B located in the meridional (peak B) and off-meridional (peak A) planes of the pattern. The higher intensity and especially reduced full width at half maximum (FWHM) of these reflections provide an estimation of an increasing length over which ordered crystalline packing is maintained as the annealing temperature increases. The longer coherence length leads finally to a reduction of the number of structural trapping sites for the charge carriers and thus to an improvement of the device performance.

2.4. Morphologies and Transport Properties

Having characterized the morphologies arising from the different molecular structure and processing (annealing, concentration and time) conditions we moved to study the effect of these morphologies on the charge carrier transport by producing OFETs based on these films. Both molecules function as p-type hole conducting channels, being at their "ON" state at negative gate-source bias. **Figure 7**a shows the output characteristics of OFETs, top contact configuration, based on **P1** oligomer with 10 mg mL^{-1} solution, annealed at four different temperatures (gate bias $V_{GS} = -10$ V). As the temperature is raised from 30 °C to 90 °C and to 120 °C the transistor performance gradually improves. At 150 °C, the current significantly drops and exhibits a clear signature of voltage-activated current often referred to as diode like curve. The evolution of the transistor characteristics can be understood with the aid of Figure 4. The subfigures (a–c) show, for films cast from the 10 mg mL^{-1} solution, that as the temperature is raised the crystals and their size become more pronounced. Namely, as the temperature is raised more amorphous material is being "collected" by the crystals that increase in size. Since the overall amount of material is limited and the density of the crystals is higher than the amorphous regions voids start to develop at higher temperature making it difficult for charges to hop between crystals. In this case the barrier to transport that is associated with the grain boundary becomes so pronounced that the current drops and becomes voltage (field) activated. This phenomena would be even more pronounced in films cast from 1 mg mL^{-1}, Figure 4d–f, where the reduced amount of available material results in clearly isolated crystals and indeed at 150 °C these "films" do not conduct at all.

Since at elevated temperatures the films cast from 1 mg mL^{-1} or 0.5 mg mL^{-1} exhibit a morphology of isolated crystal resulting at zero currents we compare in Figure 7b the performance of films cast from different solutions but annealed at same, 90 °C, temperature. Examining Figure 7a,b together with Figure 4 it is apparent that best device performance would depend on simultaneous optimization of the solution concentration and the annealing temperature.

To gain more quantitative analysis we extracted the charge (holes) carrier mobility and threshold voltage from the output curves using Equations 1a,b, where μ is the mobility, V_T is the threshold voltage, W and L are the channel width and length respectively, and C_{ox} is gate capacitance per unit of area ($C_{ox} = 35$ nF cm^{-2}).

$$\text{a)} I_{DS} = \mu \frac{W}{L} C_{ins} \left[(V_{GS} - V_T) V_{DS} - \frac{V_{DS}^2}{2} \right]$$

$$\text{b)} I_{DS} = \mu \frac{W}{2L} C_{ins} (V_{GS} - V_T)^2 \quad (1)$$

The threshold voltage and mobility were extracted first by fitting Equation 1a to the output characteristics and then by fitting Equation 1b to the transfer characteristics. To achieve good agreement between the two extraction methods one has to avoid the diode-like region and hence the parameters were extracted for high V_{DS} values with the V_{GS} values chosen according to the regime to be tested (but also high). Despite this effort to avoid "artifacts" and extract the "intrinsic" mobility it is practically impossible when the diode-like effect is very pronounced, as in the 150 °C case. Hence we enclose these values with parenthesis.

To emphasize the fact that all the parameters and their dependence on processing conditions are tightly connected to the specific chemical structure of **P1** we present in the same table also the results of the amorphous molecule **P2**. **Table 1** shows the extracted mobility (μ), threshold voltages

Table 1. OFETs parameters comparison for **P1** and **P2** thin films prepared at various annealing temperatures.

Temperature → / Molecule ↓		30 °C	90 °C	120 °C	150 °C
P1 (5 mg mL^{-1})	μ [cm^2 V^{-1} s^{-1}]	1.3×10^{-4}	5.6×10^{-4}	1.1×10^{-3}	[6.4×10^{-7}]
	V_T [V]	25	15	6	[–6]
	On-off ratio	800	2500	4500	10
P2 (5 mg mL^{-1})	μ [cm^2 V^{-1} s^{-1}]	3.3×10^{-8}	1.6×10^{-8}	2.1×10^{-8}	1.1×10^{-8}
	V_T [V]	–8	–7	–7	–9
	On-off ratio	400	500	500	400

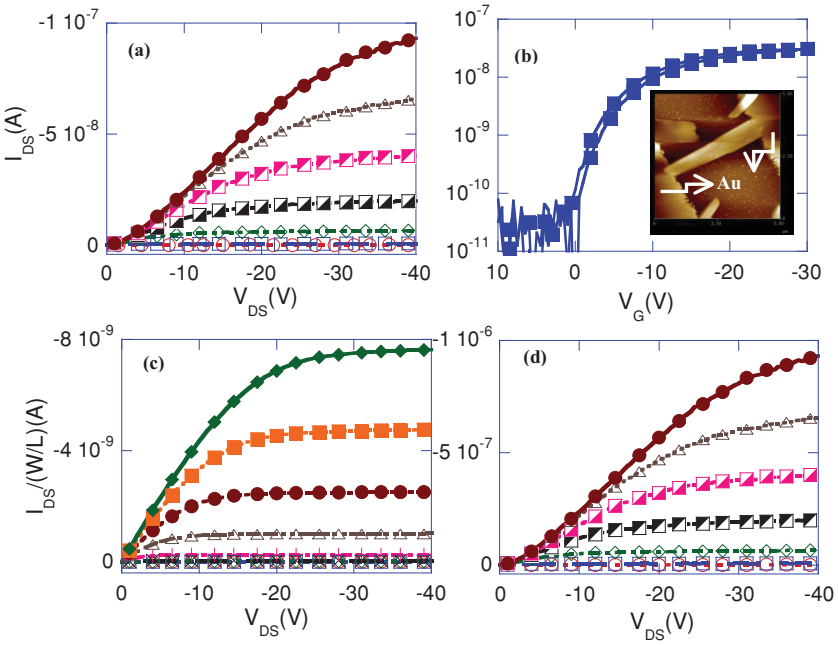

Figure 8. a) The output characteristics of **P1** single crystal OFET from V_G = 5 V to −25 V with a step size of −5 V. b) The transfer characteristic at V_{DS} = −11 V, low hysteresis is a manifestation of lower trap density. Inset of (b) shows the AFM image of single crystal between gold pads. c,d) Normalized output characteristics of best polycrystalline and a single crystal OFETs, respectively.

(V_T) and on-off ratios for both **P1** and **P2** thin films prepared with 5 mg mL^{-1} solution concentration and at four different annealing temperatures while taking into account the device to device variation (see Figure S2 and Table S2 in the Supporting Information). While the characteristics of **P2** are independent of processing conditions (and are poor) the parameters of **P1** drastically change between different conditions and we note that best reproducibility of thin film device characteristics is obtained in the temperature window of 90 °C–120 °C and solution concentration of 1–5 mg mL^{-1}. The fact that both the mobility and threshold voltage improve indicates that both the order (crystallinity) and the interface with the oxide are enhanced.

To complement the physical picture described above we also manufactured single crystal OFETs. Due to the relatively small crystal size, bottom contact configuration was used where the source and drain electrodes are defined using photolithography resulting in channel length in the 2–4 µm range. The single crystals were prepared by printing or spin coating the low concentration solution (1 mg mL^{-1}) on the prepared pattern of gold electrodes followed by annealing at 150 °C for 3 h. This procedure resulted in crystal size (length) in the 10–15 µm thus ensuring it would overlap both source and drain electrodes. While one can also use crystal transfer to locate the crystal between electrodes we preferred the direct growth of **P1** crystals on the SiO_2 substrates between the gold pads so as to maximize the process compatibility with the other FETs used. We believe that the only difference is in the contact configuration that is bottom contact for the single crystals and top contact for the films.

The inset of **Figure 8**b shows an AFM scan of the crystal as it grew between the two Au contacts. As the crystal did not grow perpendicular to the contacts edge the W and L of the single crystal device were estimated to be in the range of 400–500 nm and from 4–5 µm, respectively. The AFM picture also shows that the crystal is about the same thickness of the Au pads (≈10–20 nm) suggesting that the pads were involved in directing the growth.

The output and transfer characteristics of the crystal are shown in Figure 8a,b, respectively. The clean turn on at V_{GS} = 0 V and the low hysteresis in the transfer curve in Figure 8b are indicative of the quality of the crystal (low defects/trap density) and of the interface or the crystal surface touching the oxide. The average (taking into account device to device variation) charge carrier mobility is found to be 0.1 cm^2/Vs which is two orders of magnitude higher than that the highest mobility in thin films. The output characteristics in Figure 8a show a slight diode effect suggesting that the extracted mobility may be only slightly underestimated. To facilitate comparison to the characteristics of the films based FETs the right axis of Figure 8c,d show the current scaled to account for the difference in W/L in the two devices configurations. As the figure shows, despite the slight diode effect the maximum current (right axis) is about two orders of magnitudes higher compared to Figure 8c.

3. Conclusions

In summary, the molecules prepared using Click chemistry synthesis, which differ slightly in their structural orientation of the side groups, can exhibit either ordered, small molecules like, morphologies or amorphous, polymer-like, morphologies. A slight variation in the chemical structure is reflected in the morphological, optical, and electrical properties due to the different packing of molecules in their solid form, that is, polycrystalline and amorphous. Oligomers with side groups in plane with the molecular backbone tend to self-organize due to the larger Van der Waals interactions, resulting in high tendency towards polycrystalline films.

We emphasized here that films made of molecules with tendency to self-organize or crystallize are highly dependent on the processing conditions which include also the solution concentration and the annealing conditions (temperature and time). For the molecule tested here, best devices were obtained in the temperature window of 90–120 °C and solution concentration window of 1–5 mg mL^{-1}. This shows that the seek for (molecular) structure to (device) property relation is not trivial and a solution would be to choose the processing window in which the properties are stable and uniform and compare these properties rather than choose the best results. This study shows that in case of self arranging molecules, optimized processing conditions

lead to high performance and stable devices, whereas, in amorphous molecules processing conditions are less important.

4. Experimental Section

Materials: All the reagents and solvents described in the manuscript were of analytical grade, purchased from Sigma-Aldrich and used as received unless noted. The synthesis and characterization of P1 and P2 is described elsewhere.[13]

Film and Device Fabrication: THF was used as solvent for thin film fabrication. The films of **P1** and **P2** were spin coated (2000 rpm for 60 s) onto glass substrates for optical measurements while they were coated onto n++Si/SiO_2(100 nm) substrates for AFM measurements and OFETs. Films were annealed at different temperatures for studying different morphologies under rough vacuum. Single crystal devices were fabricated on already patterned gold n++Si/SiO_2 substrates, the pattering was done by photolithography technique. 1–0.5 mg mL^{-1} solution was printed on the desired area and then annealed at 150 °C for 3 h in rough vacuum.

Measurements: Optical absorption spectra of solution (THF) and films were measured with a UV-visible-NIR spectrophotometer (UV-3101PC Shimadzu). Grazing angle X-ray was used to measure X-ray diffraction (XRD) with the Rikagu SmartLab high-resolution diffraction system. A surface profiler (Dektak 150) was used to measure film thicknesses. The nanostructure growth of **P1** films was measured using a grazing incidence wide-angle X-ray scattering (GIWAXS) system (Max Planck Institute for Polymer Research, Germany), while their surface morphologies were measured with an atomic force microscope (AFM) system (NanoscopeIIIa, Digital Instruments). OFET measurements were done under inert atmosphere by Agilent 1500A Semiconductor Device Analyzer.

Supporting Information

Supporting Information is available from the Wiley Online Library or from the author.

Acknowledgements

This work was financially supported by CommonSense FP7 grants and by the Technion funds for security research.

Received: October 19, 2013
Published online: January 6, 2014

[1] a) C. W. Tang, S. A. Vanslyke, *Appl. Phys. Lett.* **1987**, *51*, 913; b) J. H. Burroughes, D. D. C. Bradley, A. R. Brown, R. N. Marks, K. Mackay, R. H. Friend, P. L. Burns, A. B. Holmes, *Nature* **1990**, *347*, 539.
[2] D. W. Samuel, G. A. Turnbull, *Chem. Rev.* **2007**, *107*, 1272.
[3] a) Z. Bao, J. Locklin, Organic Field-Effect Transistors, 1st ed., CRC Press, Boca Raton, FL, **2007**; b) C. D. Dimitropoulos, L. P. R. Malenfant, *Adv. Mater.* **2002**, *14*, 99.
[4] a) S. Ravishankar, B. Dudhea, S. Jasmine, A. Kumar, V. R. Rao, *Sens. Actuators B* **2010**, *148*, 158; b) Y. Gannot, C. Hertzog-Ronen, N. Tessler, Y. Eichen, *Adv. Funct. Mater.* **2010**, *20*, 105; c) Y. Eichen, Y. Gerchikov, E. Borzin, Y. Gannot, A. Shemesh, S. Meltzman, C. Hertzog-Ronen, S. Tal, S. Stolyarova, Y. Nemirovsky, N. Tessler, Sensor Arrays (Ed: W. Yang), ISBN: 978–953–51–0613–5, **2012**; d) Y. Gerchikov, E. Borzin, Y. Gannot, A. Shemesh, S. Meltzman, C. Hertzog-Ronen, S. Tal, S. Stolyarova, Y. Nemirovsky, Nir Tessler, Y. Eichen, *J. Phys.: Conf. Series* **2011**, *307*, 012020.
[5] a) C. Brabec, V. Dyakonov, U. Scherf, Organic Photovoltaics; Materials, Device Physics, and Manufacturing Technologies, Wiley-VCH, Weinheim **2008**; b) T. A. Skotheim, R. L. Elsenbaumer, J. R. Reynolds, Handbook of Conducting Polymers Marcel Dekker, New York **1998**.
[6] P. Kumar, A. Sharma, S. Yadav, S. Ghosh, *Org. Electron.* **2013**, *14*, 1663.
[7] H. Sirringhaus, *Adv. Mater.* **2005**, *17*, 2411.
[8] H. N. Tsao, D. M. Cho, I. Park, M. R. Hansen, A. Mavrinskiy, D. Y. Yoon, R. Graf, W. Pisula, H. W. Spiess, K. Müllen et al. *J. Am. Chem. Soc.* **2011**, *133*, 2605.
[9] T. Maddux, W. Li, L. Yu, *J. Am. Chem. Soc.* **1997**, *119*, 844.
[10] M. Jorgensen, F. C. Krebs, *J. Org. Chem.* **2004**, *69*, 6688.
[11] a) M. Firstenberg, K. N. Shivananda, I. Cohen, O. Solomeshch, V. Medvedev, N. Tessler, Y. Eichen, *Adv. Funct. Mater.* **2011**, *21*, 634; b) H. C. Kolb, M. G. Finn, K. B. Sharpless, *Angew. Chem.* **2001**, *40*, 2004.
[12] a) N. Tessler, O. Globerman, N. Rappaport, Y. Preezant, Y. Roichman, O. Solomesch, J. Veres, S. Tal, E. Gershman, M. Adler, V. Zolotarev, V. Gorelik, Y. Eichen, in Conjugated Polymers: Processing and Applications (Handbook of Conducting Polymers 3rd Edition) (Eds: T. A. Skotheim, J. Reynolds), CRC Press, Boca Raton, Florida **2006**, Ch. 7; b) O. Solomeshch, Y. J. Yu, V. Medvedev, A. Razin, B. Blumer-Ganon, Y. Eichen, J. I. Jin, N. Tessler, *Synth. Met.* **2007**, *157*, 841.
[13] K. N. Shivananda, I. Cohen, E. Borzin, Y. Gerchikov, M. Firstenberg, O. Solomeshch, N. Tessler, Y. Eichen, *Adv. Funct. Mater.* **2012**, *22*, 1489.
[14] H. Proehl, T. Dienel, R. Nitsche, T. Fritz, *Phys. Rev. Lett.* **2004**, *93*, 097403.